$$\begin{aligned}
&\mathbf{A}\,\mathbf{B}\,\mathbf{C}+\mathbf{B}\,\mathbf{C}\,\mathbf{A}+\mathbf{C}\,\mathbf{A}\,\mathbf{B}+\mathbf{C}\,\mathbf{B}\,\mathbf{A}+\mathbf{A}\,\mathbf{C}\,\mathbf{B}+\mathbf{B}\,\mathbf{A}\,\mathbf{C}\\
&\quad=\{\mathrm{tr}(\mathbf{A})\,\mathrm{tr}(\mathbf{B})\,\mathrm{tr}(\mathbf{C})-\mathrm{tr}(\mathbf{A})\,\mathrm{tr}(\mathbf{B}\,\mathbf{C})-\mathrm{tr}(\mathbf{B})\,\mathrm{tr}(\mathbf{C}\,\mathbf{A})-\mathrm{tr}(\mathbf{C})\,\mathrm{tr}(\mathbf{A}\,\mathbf{B})\\
&\quad+\mathrm{tr}(\mathbf{A}\,\mathbf{B}\,\mathbf{C})+\mathrm{tr}(\mathbf{A}\,\mathbf{C}\,\mathbf{B})\}\,\mathbf{1}\\
&\quad-\{\mathrm{tr}(\mathbf{B})\,\mathrm{tr}(\mathbf{C})-\mathrm{tr}(\mathbf{B}\,\mathbf{C})\}\,\mathbf{A}-\{\mathrm{tr}(\mathbf{C})\,\mathrm{tr}(\mathbf{A})-\mathrm{tr}(\mathbf{C}\,\mathbf{A})\}\,\mathbf{B}\\
&\quad-\{\mathrm{tr}(\mathbf{A})\,\mathrm{tr}(\mathbf{B})-\mathrm{tr}(\mathbf{A}\,\mathbf{B})\}\,\mathbf{C}\\
&\quad+\mathrm{tr}(\mathbf{A})\,(\mathbf{B}\,\mathbf{C}+\mathbf{C}\,\mathbf{B})+\mathrm{tr}(\mathbf{B})\,(\mathbf{C}\,\mathbf{A}+\mathbf{A}\,\mathbf{C})+\mathrm{tr}(\mathbf{C})\,(\mathbf{A}\,\mathbf{B}+\mathbf{B}\,\mathbf{A})\,. \qquad (1.4.2)
\end{aligned}$$

Substitution of $\mathbf{B}=\mathbf{C}=\mathbf{A}$ into (1.4.2) yields the Hamilton-Cayley theorem, (1.2.11). In this theorem, *tensor* $\mathbf{A}$ *need not be symmetric.*

Substituting $\mathbf{C}=\mathbf{A}$ into (1.4.2), obtain another identity relating two second-order arbitrary tensors $\mathbf{A}$ and $\mathbf{B}$,

$$\begin{aligned}
&\mathbf{A}\,(\mathbf{A}\,\mathbf{B}+\mathbf{B}\,\mathbf{A})+(\mathbf{A}\,\mathbf{B}+\mathbf{B}\,\mathbf{A})\,\mathbf{A}-\mathrm{I}_{\mathbf{A}}\,(\mathbf{A}\,\mathbf{B}+\mathbf{B}\,\mathbf{A})+\mathrm{II}_{\mathbf{A}}\,\mathbf{B}-\mathbf{A}\,\mathbf{B}\,\mathbf{A}\\
&\quad=\mathrm{tr}(\mathbf{B})\,\mathbf{A}^2+\{\mathrm{tr}(\mathbf{A}\,\mathbf{B})-\mathrm{I}_{\mathbf{A}}\,\mathrm{tr}(\mathbf{B})\}\,\mathbf{A}\\
&\quad+\{\mathrm{tr}(\mathbf{A}^2\,\mathbf{B})-\mathrm{I}_{\mathbf{A}}\,\mathrm{tr}(\mathbf{A}\,\mathbf{B})+\mathrm{II}_{\mathbf{A}}\,\mathrm{tr}(\mathbf{B})\}\,\mathbf{1}\,. \qquad (1.4.3)
\end{aligned}$$

Replace $\mathbf{B}$ in (1.4.3) by $\mathbf{A}\,\mathbf{B}+\mathbf{B}\,\mathbf{A}$, and use the Hamilton-Cayley theorem to arrive at another identity,

$$\begin{aligned}
&\mathbf{A}\,(\mathbf{A}\,\mathbf{B}+\mathbf{B}\,\mathbf{A})\,\mathbf{A}+\mathrm{III}_{\mathbf{A}}\,\mathbf{B}-\mathrm{I}_{\mathbf{A}}\,\mathbf{A}\,\mathbf{B}\,\mathbf{A}\\
&\quad=\mathrm{tr}(\mathbf{A}\,\mathbf{B})\,\mathbf{A}^2+\{\mathrm{tr}(\mathbf{A}^2\,\mathbf{B})-\mathrm{I}_{\mathbf{A}}\,\mathrm{tr}(\mathbf{A}\,\mathbf{B})\}\,\mathbf{A}+\mathrm{III}_{\mathbf{A}}\,\mathrm{tr}(\mathbf{B})\,\mathbf{1}\,. \qquad (1.4.4)
\end{aligned}$$

Similarly, replace $\mathbf{B}$ in (1.4.3) by $\mathbf{A}\,\mathbf{B}\,\mathbf{A}$ to obtain

$$\begin{aligned}
&\mathbf{A}^2\,\mathbf{B}\,\mathbf{A}^2+\mathrm{III}_{\mathbf{A}}\,(\mathbf{A}\,\mathbf{B}+\mathbf{B}\,\mathbf{A})-\mathrm{II}_{\mathbf{A}}\,\mathbf{A}\,\mathbf{B}\,\mathbf{A}\\
&\quad=\mathrm{tr}(\mathbf{A}^2\,\mathbf{B})\,\mathbf{A}^2+\{\mathrm{III}_{\mathbf{A}}\,\mathrm{tr}(\mathbf{B})-\mathrm{II}_{\mathbf{A}}\,\mathrm{tr}(\mathbf{A}\,\mathbf{B})\}\,\mathbf{A}+\mathrm{III}_{\mathbf{A}}\,\mathrm{tr}(\mathbf{A}\,\mathbf{B})\,\mathbf{1}\,. \qquad (1.4.5)
\end{aligned}$$

Identities (1.4.2) to (1.4.5) are referred to as Rivlin's identities.

1.4.2. Other Related Identities

Eliminate the term $\mathbf{A}\,\mathbf{B}\,\mathbf{A}$ from (1.4.3) and (1.4.4) to arrive at

$$\begin{aligned}
&(\mathrm{I}_{\mathbf{A}}\,\mathrm{II}_{\mathbf{A}}-\mathrm{III}_{\mathbf{A}})\,\mathbf{B}=\mathbf{A}\,(\mathbf{A}\,\mathbf{B}+\mathbf{B}\,\mathbf{A})\,\mathbf{A}+\mathrm{I}_{\mathbf{A}}^2\,(\mathbf{A}\,\mathbf{B}+\mathbf{B}\,\mathbf{A})\\
&\quad-\mathrm{I}_{\mathbf{A}}\,\{\mathbf{A}\,(\mathbf{A}\,\mathbf{B}+\mathbf{B}\,\mathbf{A})+(\mathbf{A}\,\mathbf{B}+\mathbf{B}\,\mathbf{A})\,\mathbf{A}\}+\{\mathrm{I}_{\mathbf{A}}\,\mathrm{tr}(\mathbf{B})-\mathrm{tr}(\mathbf{A}\,\mathbf{B})\}\,\mathbf{A}^2\\
&\quad-\{\mathrm{I}_{\mathbf{A}}^2\,\mathrm{tr}(\mathbf{B})-2\,\mathrm{I}_{\mathbf{A}}\,\mathrm{tr}(\mathbf{A}\,\mathbf{B})+\mathrm{tr}(\mathbf{A}^2\,\mathbf{B})\}\,\mathbf{A}\\
&\quad+\mathrm{III}_{\mathbf{A}}\,\{\mathrm{I}_{\mathbf{A}}\,\mathrm{tr}(\mathbf{A}^{-1}\,\mathbf{B})-\mathrm{tr}(\mathbf{B})\}\,\mathbf{1}\,. \qquad (1.4.6)
\end{aligned}$$

Following Scheidler (1994), express identity (1.4.6) as

$$\begin{aligned}
\mathrm{III}_{\tilde{\mathbf{A}}}\,\mathbf{B}&=\tilde{\mathbf{A}}\,(\mathbf{A}\,\mathbf{B}+\mathbf{B}\,\mathbf{A})\,\tilde{\mathbf{A}}+\mathrm{tr}(\tilde{\mathbf{A}}\,\mathbf{B})\,\mathbf{A}^2-\mathrm{tr}(\tilde{\mathbf{A}}^2\,\mathbf{B})\,\mathbf{A}\\
&\quad+\mathrm{III}_{\mathbf{A}}\,\mathrm{tr}(\mathbf{A}^{-1}\,\tilde{\mathbf{A}}\,\mathbf{B})\,\mathbf{1}\,, \qquad (1.4.7a)
\end{aligned}$$

with

obtain a coordinate-independent expression for the material time derivative of the logarithmic strain. Scheidler (1991a) provides an alternative proof for Hill's (1978) formula when the principal stretches are repeated. Scheidler (1991b) then gives approximate coordinate-independent formulae for the time derivatives of the generalized strain tensors.

Thus, the isotropic tensor-valued functions of symmetric second-order tensors and their time derivatives, have received considerable attention in the kinematics of finite deformation. Those of nonsymmetric tensors seem to have been addressed only recently. In this section, exact explicit coordinate-independent expressions are given for a class of isotropic tensor-valued functions of nonsymmetric second-order tensors, following Balendran and Nemat-Nasser (1996).

1.5.1. A Class of Isotropic Tensor-valued Functions of Real-valued Second-order Tensors

Let f(x) be a suitably differentiable function, admitting a uniformly convergent Taylor series expansion. Then, to any desired degree of accuracy, f(x) can be represented by

$$f(x) = \sum_{m=0}^{n} \alpha_m x^m , \tag{1.5.1a}$$

where α_i's are constants, and n is a suitable large integer. Consider a class of tensor-valued functions $\mathbf{f}(\mathbf{A})$ that can be expressed as follows:

$$\mathbf{f}(\mathbf{A}) = \sum_{m=0}^{n} \alpha_m \mathbf{A}^m . \tag{1.5.1b}$$

This tensor-valued function is isotropic. Hence,

$$\mathbf{f}(\mathbf{R}^T \mathbf{A}\, \mathbf{R}) = \mathbf{R}^T \mathbf{f}(\mathbf{A})\, \mathbf{R} ,$$

for any proper orthogonal (rotation) tensor $\mathbf{R}$. At focus here is the class (1.5.1b) of isotropic tensor-valued functions of any real-valued second-order tensor with distinct, repeated, or complex-valued eigenvalues.

Substituting the coordinate-independent expressions for $\mathbf{A}^m$, m = 1, 2, ..., n, from (1.3.17d), (1.3.22d), and (1.3.25a) into (1.5.1b), obtain

$$\mathbf{f}(\mathbf{A}) = \mathbf{f}(\bar{\mathbf{A}}) + f'(\lambda)\, \mathbf{L} + \frac{1}{2} f''(\lambda)\, \mathbf{L}^2 , \tag{1.5.2a}$$

should not be bold

where

$$\mathbf{f}(\bar{\mathbf{A}}) = \sum_{m=0}^{n} \alpha_m \bar{\mathbf{A}}^m , \qquad \bar{\mathbf{A}} = \mathbf{A} - \mathbf{L} , \tag{1.5.2b,c}$$

$$\mathbf{L} = \mathbf{0} , \quad \text{for } \lambda_1 \neq \lambda_2 \neq \lambda_3 \neq \lambda_1 ,$$

---

[11] See Subsection 2.10.2, page 84.

$$\tau = \tau_a + \tau^* + \tau_d\,, \qquad \tau_d = m_0\,[1 - \exp(-\alpha\dot{\gamma})], \tag{4.8.21a,b}$$

where m_0 is a constant, and, in the range of the considered strain rates, $\alpha = O(10^{-4})$s. In this case, expansion of the exponential term in Taylor series gives,

$$\tau_d \approx m_0\,\alpha\dot{\gamma}\,, \tag{4.8.21c}$$

so that, in view of (4.8.20d,e), it follows that[81]

$$\alpha \approx \frac{D}{m_0\, b^2\, \rho_m}\,. \tag{4.8.21d}$$

4.8.9. Application: Flow Stress of Commercially Pure Tantalum

Consider as illustration, applying the physically-based model (4.8.11) with τ_a defined by (4.8.18b) to tantalum (Ta) which is a bcc metal. To simplify the analysis, neglect the influence of the grain size, and use, for the athermal part of the flow stress,

$$\tau_a = c_0 + c_1\,\gamma^{n_1}\,, \tag{4.8.18e}$$

where c_0 and c_1 are to be fixed empirically.

For bcc metals, the lattice itself provides the short-range barrier (the Peierls barrier) to the motion of dislocations. Generally, a double kink is formed with the assistance of thermal vibrations, and the kinks then move sideways, leading to the advancement of the dislocation line. In this process, the kinks may be pinned down by other defects or alloying elements, thereby increasing the resistance to the plastic deformation. For tantalum-tungsten (Ta-W) alloys, the (substitutional) tungsten atoms may pin down the kinked dislocations in their lateral motion. Hence, the flow stress for Ta-W is generally higher than that for commercially pure tantalum (Nemat-Nasser and Kapoor, 2001). In what follows, the thermally activated part of the flow stress is assumed to correspond solely to the Peierls resistance to the dislocation motion. The results, therefore, are applicable to, for example, commercially pure tantalum, molybdenum, niobium, and vanadium; see Table 4.8.1, page 235, for the values of their constitutive parameters.

Modified Hopkinson experimental techniques have been used to measure the flow stress of ductile materials over a broad range of strains, strain rates, and temperatures, in uniaxial stress.[82] Figure 4.8.3 gives the adiabatic flow stress of commercially pure tantalum tested in compression at a 5,000/s strain rate and at

---

[81] If m_0 is identified with the material's yield stress at a suitably high temperature, say, about 1,000K, and the Taylor factor M is also introduced, then equation (4.8.21d) corresponds to equation $(3.6)_2$ of Nemat-Nasser *et al.* (2001a).

[82] Nemat-Nasser *et al.* (1991), Nemat-Nasser and Isaacs (1997a,b), Nemat-Nasser (2000b), and *ASM Volume 8* (2000).

rates. The constitutive parameters of several refractory metals that have been experimentally characterized, are listed in Table 4.8.1.

Finally, note that, in (4.8.22e), the thermal component of the flow stress is *non-negative*, and should be set equal to zero when the temperature exceeds a corresponding critical value which is strain-rate dependent, and which is given by

$$T_c = \left\{ \frac{k}{G_0} \, ln \frac{\dot{\gamma}_r}{\dot{\gamma}} \right\}^{-1} . \qquad \text{Location of left brace moved} \qquad (4.8.22f)$$

For $\dot{\gamma} = 10^{-3}$, 10^{-1}, 1,000, 5,000, and 40,000/s, this gives, $T_c =$ 430, 520, 880, 1,000, and 1,220K, respectively.

Table 4.8.1

Values of constitutive parameters in (4.8.22e) for indicated commercially pure metals[a]

	p	q	k/G_0 10^{-5}K	$\dot{\gamma}_r$ 10^7	$\hat{\tau}$ MPa	c_1 MPa	n_1
Ta	2/3	2	8.62	54.6	1,100	473	1/5
Va	2/3	2	17.2	0.357	1,050	305	1/5
Nb	2/3	2	12.4	0.35	1,680	440	1/4
Mo	2/3	2	8.62	1.45	2,450	720	1/4

value corrected

[a] It is assumed that $c_0 \approx 0$ in all cases.

Application to Molybdenum: As pointed out before, the model predicts experimental results obtained for commercially pure molybdenum, as reported by Nemat-Nasser *et al.* (1999b). The corresponding parameters are given in Table 4.8.1. Figure 4.8.9 shows some of the results obtained by these authors for a 3,100/s strain rate and indicated initial temperatures. For the model calculation, it is assumed that the entire plastic work is used to heat the sample. The sample temperature is estimated using (4.8.22d), with $(\hat{\rho}\, C_v)^{-1} \approx 0.39$K/MPa. Figure 4.8.10 compares the experimental results for an 8,000/s strain rate and indicated initial temperatures, with the corresponding model predictions.

4.8.10. Application to OFHC Copper

Consider applying the model of (4.8.5a) with the thermally activated part of the flow stress given by (4.8.15a) and the athermal part defined by (4.8.18d), to predict the response of OFHC copper deformed in compression at various strain rates and temperatures. To simplify the modeling, neglect the grain-size effect, use the approximation (4.8.12p,q) with $n_0 = 1/2$, $q = 2$, and $p = 2/3$, and consider the following semi-empirical form of the basic equations:

$$\dot{\gamma} = \frac{1}{H} \frac{\partial f}{\partial \boldsymbol{\tau}} : \overset{\circ}{\boldsymbol{\tau}}' \tag{4.9.39b}$$

where the workhardening parameter H is defined by

$$H = -\left\{ \frac{\partial f}{\partial \gamma} + \frac{\partial f}{\partial \boldsymbol{\beta}} \cdot \frac{d\boldsymbol{\beta}}{d\gamma} \right\}. \tag{4.9.39c}$$

Given $\mathbf{D}$ and $\mathbf{W}$, (4.9.38a) must be integrated together with the evolution equations (4.9.3), to obtain the stress increment and the increments in the internal variables $\boldsymbol{\beta}$, over a suitable time interval, as discussed in Chapter 5. For this, it is necessary to calculate $\mathbf{L}^{e\Omega} = \mathbf{L}^e + \boldsymbol{\Omega}$, in order to obtain an expression for the objective stress rate $\overset{\nabla}{\boldsymbol{\tau}}{}^{e\Omega}$, (4.9.31d). In principle, this is always possible, although the presence of the elastic deformation, *i.e.,* the term $\mathbf{V}^e$, in the kinematical equations complicates the details. The elastic strains are, however, usually very small. If this fact is used, then the expressions simplify considerably, as is discussed in the sequel, after the general case is outlined.

Without regard for the smallness of the elastic strains, based on (4.9.7a-d) note that $\mathbf{W}^p$ is given as a homogeneous and linear function of $\mathbf{D}^p$. Indeed, from $\overline{\mathbf{D}}^p + \overline{\mathbf{W}}^p = \mathbf{V}^{e-1} (\mathbf{D}^p + \mathbf{W}^p) \mathbf{V}^e$ and the relation between $\overline{\mathbf{W}}^p$ and $\overline{\mathbf{D}}^p$, *i.e.*, (4.9.21a), obtain

$$\{\mathbf{V}^{e-1} (\mathbf{D}^p + \mathbf{W}^p) \mathbf{V}^e\}_{skew} = \mathfrak{K}(\overline{\mathbf{U}}^p) : \{\mathbf{V}^{e-1} (\mathbf{D}^p + \mathbf{W}^p) \mathbf{V}^e\}_{sym}, \tag{4.9.40}$$

where the subscripts skew and sym denote the skewsymmetric and the symmetric parts of the corresponding expression. Since $\mathbf{D}^p$ is defined by the constitutive relation (4.9.2), expression (4.9.40) gives $\mathbf{W}^p$ as a linear function of $\dot{\gamma}\, \partial g/\partial \boldsymbol{\tau}$. Once $\mathbf{W}^p$ is defined in this manner, $\mathbf{W}^{e\Omega} = \mathbf{W} - \mathbf{W}^p$ and hence, $\mathbf{L}^{e\Omega} = \mathbf{W}^{e\Omega} + (\mathbf{D} - \mathbf{D}^p)$, are expressed as linear functions of $\dot{\gamma}\, \partial g/\partial \boldsymbol{\tau}$. With these expressions, the left-hand side of (4.9.38a) is defined in terms of $\dot{\boldsymbol{\tau}}$, $\boldsymbol{\tau}$, and $\dot{\gamma}\, \partial g/\partial \boldsymbol{\tau}$. The resulting differential equation can hence be integrated numerically to obtain the stress increment.

4.9.8. Small Elastic Deformations

To make the above results transparent, examine the consequences of the fact that the elastic strains are usually very small, say, less than 1% for most metals. Set

$$\mathbf{V}^e = \mathbf{1} + \boldsymbol{\varepsilon}, \qquad \mathbf{V}^{e-1} = \mathbf{1} - \boldsymbol{\varepsilon} + O(\boldsymbol{\varepsilon}^2), \tag{4.9.41a,b}$$

where $O(\boldsymbol{\varepsilon}^2)$ denotes terms of the order of $\boldsymbol{\varepsilon}^2$ and greater. Note that, if $|\boldsymbol{\varepsilon}|$ is of the order of 0.01, then $|\boldsymbol{\varepsilon}^2|$ would be of the order of 0.0001. The plastic strains and rigid-body rotations of material elements, on the other hand, are usually rather large. From $\overline{\mathbf{L}} = \mathbf{V}^{e-1} \mathbf{L}^p \mathbf{V}^e$ and (4.9.41a,b), it follows that

$$\begin{aligned} \overline{\mathbf{W}}^p &= \mathbf{W}^p - \boldsymbol{\varepsilon}\, \mathbf{D}^p + \mathbf{D}^p \boldsymbol{\varepsilon} + O(\boldsymbol{\varepsilon}^2), \\ \overline{\mathbf{D}}^p &= \mathbf{D}^p - \boldsymbol{\varepsilon}\, \mathbf{W}^p + \mathbf{W}^p \boldsymbol{\varepsilon} + O(\boldsymbol{\varepsilon}^2). \end{aligned} \tag{4.9.42a,b}$$

$$\mathbf{R}_t = \mathbf{F}_t \mathbf{U}_t^{-1} . \qquad (5.2.25a\text{-}l)$$

Note that, the evaluation of the tensors $\mathbf{C}_t$ and $\mathbf{C}_t^2$ and the coefficients k, a, and b, requires 88 floating point operations. With an additional 14 floating point operations, and 1, 3, and 4, evaluations of *arc cosine*, *cosine*, and *square root*, respectively, the principal stretches can be obtained. Then the invariants of the stretch tensor $\mathbf{U}_t$ require 9 more floating point operations. Evaluation of $\mathbf{U}_t^{-1}$ and $\mathbf{R}_t$ requires 21 and 45 floating point operations, respectively. In total, 186 floating point operations, and 1, 3, and 4 evaluations of *arc cosine*, *cosine*, and *square root*, respectively, are required to determine the rotation tensor *exactly*. Rashid's (1993) *approximate* estimate requires 105 floating point operations and 2 evaluations of *square root*.

Using (5.2.12), the constant corotational deformation rate is evaluated *exactly*, where (5.2.27) is obtained from (1.5.14) and (1.5.15):

(i) $a = 0$

$$\hat{\mathbf{D}} = \frac{ln(\lambda_1)}{\Delta t} \mathbf{1} . \qquad (5.2.26)$$

(ii) $a^3 = b^2 \neq 0$

$$\hat{\mathbf{D}} = \frac{ln(\lambda_1) - ln(\lambda_2)}{(\lambda_1^2 - \lambda_2^2)\Delta t} \mathbf{C}_t + \frac{\lambda_1^2 ln(\lambda_2) - \lambda_2^2 ln(\lambda_1)}{(\lambda_1^2 - \lambda_2^2)\Delta t} \mathbf{1} . \qquad (5.2.27)$$

removed exponent 2

(iii) $a^3 \neq b^2$

$$\Delta = -(\lambda_1^2 - \lambda_2^2)(\lambda_2^2 - \lambda_3^2)(\lambda_3^2 - \lambda_1^2) ,$$

$$\begin{bmatrix} a_0 \\ -a_1 \\ a_2 \end{bmatrix} = \frac{1}{\Delta} \begin{bmatrix} \lambda_2^2\lambda_3^2 & \lambda_3^2\lambda_1^2 & \lambda_1^2\lambda_2^2 \\ \lambda_2^2 + \lambda_3^2 & \lambda_3^2 + \lambda_1^2 & \lambda_1^2 + \lambda_2^2 \\ 1 & 1 & 1 \end{bmatrix} \begin{bmatrix} ln(\lambda_1)(\lambda_2^2 - \lambda_3^2) \\ ln(\lambda_2)(\lambda_3^2 - \lambda_1^2) \\ ln(\lambda_3)(\lambda_1^2 - \lambda_2^2) \end{bmatrix} ,$$

$$\hat{\mathbf{D}} = \frac{1}{\Delta t}(a_0 \mathbf{1} + a_1 \mathbf{C}_t + a_2 \mathbf{C}_t^2) . \qquad (5.2.28a\text{-}c)$$

This requires a maximum of 32 floating point operations and 3 evaluations of *logarithm*. The approximate expression in Rashid's procedure requires an additional 52 floating point operations.

Summarizing, the *exact* evaluation of $\mathbf{R}_t$ and $\hat{\mathbf{D}}$ for a given $\mathbf{F}_t$, requires 218 floating point operations and 1, 3, 4, and 3, evaluations of *arc cosine*, *cosine*, *square root*, and *logarithm*, respectively. The *approximate* evaluation of $\mathbf{R}_t$ and $\hat{\mathbf{D}}$ for a given $\mathbf{F}_t$, requires 157 floating point operations and 2 evaluations of *square root*. As shown by Rashid (1993), the approximate expressions $\hat{\mathbf{D}}^R$ and $\mathbf{R}_t^R$ are accurate only to the second and first order of $\mathbf{U}_t - \mathbf{1}$, respectively.

$$\tau_A = F(\gamma_A), \quad \Delta\beta_A = \int_{\gamma(t)}^{\gamma_A} \Lambda(\gamma)\, d\gamma,$$
$$H_A = H(\gamma_A), \quad \Lambda_A = \Lambda(\gamma_A). \tag{5.7.17a-f}$$

Step 5

Estimate the error in the plastic strain increment and correct,

$$\Delta\gamma_{er} = \frac{\tau_A - \tau_y(t) + \Delta\beta_A}{\mu + H_A + \Lambda_A}, \quad \Delta\gamma = \Delta\gamma_A - \Delta\gamma_{er}. \tag{5.7.18a,b}$$

Step 7

Obtain the final values of the equivalent plastic strain, total stress, and the back-stress,

$$\gamma(t+\Delta t) = \gamma(t) + \Delta\gamma,$$
$$\hat{\boldsymbol{\tau}}(t+\Delta t) = \left\{ 1 - \frac{\mu \Delta\gamma}{\tau^{tr}} \right\} \hat{\mathbf{s}}^{tr} + \hat{\boldsymbol{\beta}}(t),$$
$$\hat{\boldsymbol{\beta}}(t+\Delta t) = \hat{\boldsymbol{\beta}}(t) + (\Delta\beta_A - \Lambda_A \Delta\gamma_{er}) \frac{\hat{\mathbf{s}}^{tr}}{\tau^{tr}}. \tag{5.7.19a-c}$$

Note that, if $\tau^{\alpha} \le \tau_y(t)$, then from (5.7.12), $\Delta t^p = 0$ and $\hat{\mathbf{s}}^{tr} = \hat{\mathbf{s}}^{\alpha}$. Hence, from (5.7.17a), $\Delta\gamma_A = 0$. This yields $\Delta\beta_A = 0$ and $\tau_A = \tau_y(t)$, and from (5.7.18a), $\Delta\gamma_{er} = 0$. In this case, the final values are given by

$$\hat{\boldsymbol{\tau}}(t+\Delta t) = \hat{\mathbf{s}}^{\alpha} + \hat{\boldsymbol{\beta}}(t), \quad \hat{\boldsymbol{\beta}}(t+\Delta t) = \hat{\boldsymbol{\beta}}(t). \tag{5.7.19d,e}$$

Thus, the method produces exact results for elastic deformation. The time required to reach the yield surface is not explicitly calculated. This fact renders the *generalized radial-return method* very attractive for implementation in large-scale computer codes. *The generalization outlined above ensures that the objectivity is satisfied in the presence of isotropic and kinematic hardening, including the noncoaxiality effect. Furthermore, the use of the plastic-predictor/elastic-corrector method, ensures that the stress magnitude is calculated almost exactly in one step.*

Example: As an illustration consider an isotropic hardening with yield function

$$F(\gamma) = \tau_c (1 + \gamma/\gamma_0)^N, \tag{5.7.20a}$$

where $\tau_c = \mu/100$, $\gamma_0 = 0.005$, and $N = 0.1$. As an example consider the following time history for the corotational deformation rate $\hat{\mathbf{D}}$:

$$\hat{\mathbf{D}} = \begin{bmatrix} 1 & 0 & 0 \\ 0 & -1 & 0 \\ 0 & 0 & 0 \end{bmatrix} \times 10^{-2}, \quad 0 \le t < 50,$$
$$\hat{\mathbf{D}} = \begin{bmatrix} 1 & 1 & 0 \\ 1 & -1 & 0 \\ 0 & 0 & 0 \end{bmatrix} \times 10^{-2}, \quad 50 \le t < 100,$$

Step 2

In the absence of noncoaxiality, obtain the trial stress difference, and its magnitude and then correct for noncoaxiality,

$$\hat{\mathbf{s}}^{\alpha} = \hat{\mathbf{s}}(t) + 2\mu\,\hat{\mathbf{D}}\,\Delta t\,, \qquad \tau^{\alpha} = (\tfrac{1}{2}\,\hat{\mathbf{s}}^{\alpha} : \hat{\mathbf{s}}^{\alpha})^{1/2}\,.$$

$$\hat{\mathbf{s}}^{tr} = \hat{\mathbf{s}}^{\alpha} + \mu\,\bar{\alpha}\,\{2\,\hat{\mathbf{D}} - (\hat{\mathbf{s}}^{\alpha} : \hat{\mathbf{D}})\,\hat{\mathbf{s}}^{\alpha}/(\tau^{\alpha})^2\}\,\Delta t^{p}\,,$$

$$\tau^{tr} = (\tfrac{1}{2}\,\hat{\mathbf{s}}^{tr} : \hat{\mathbf{s}}^{tr})^{1/2}\,. \tag{5.7.45a-d}$$

Step 3

Calculate the effective initial stress and deformation rate,

$$s_t = \frac{\hat{\mathbf{s}}(t) : \hat{\boldsymbol{\mu}}^{tr}}{\sqrt{2}}\,, \qquad \dot{\varepsilon} = \frac{\tau^{tr} - s_t}{\mu\,\Delta t}\,, \qquad \hat{\boldsymbol{\mu}}^{tr} = \frac{\hat{\mathbf{s}}^{tr}}{\sqrt{2}\,\tau^{tr}}\,. \tag{5.7.46a-c}$$

Step 4

If $\dot{\varepsilon} < 0$, then set $\Delta\gamma = \Delta\beta = 0$ and go to Step 8.

Step 5

Calculate the initial effective estimated plastic strain rate, and the final flow stress from the flow rule,

$$\dot{\varepsilon}_t^{p} = \text{sign}(s_t)\,g(|\,s_t\,|\,,\ \gamma(t))\,,$$

$$\tau_d = F(\dot{\varepsilon},\ \gamma(t))\,. \tag{5.7.47a,b}$$

Step 6

Estimate the plastic strain increment, plastic strain rate, and the effective stress at the end of the timestep,

$$k = \mu\,\frac{\dot{\varepsilon} - \dot{\varepsilon}_t^{p}}{\tau_d - s_t}\,,$$

$$\Delta\gamma_A = \dot{\varepsilon}\,\Delta t - \frac{\tau_d - s_t}{\mu}\,(1 - e^{-k\Delta t})\,,$$

$$\dot{\gamma}_A = \dot{\varepsilon} - (\dot{\varepsilon} - \dot{\varepsilon}_t^{p})\,e^{-k\Delta t}\,,$$

$$\tau^{e} = s_t + (\tau_d - s_t)\,(1 - e^{-k\Delta t})\,. \tag{5.7.48a-d}$$

Step 7

Estimate the flow stress, the increment in the backstress, and the hardening moduli,

$$\gamma_A = \gamma(t) + \Delta\gamma_A\,, \qquad \tau_A = F(\dot{\gamma}_A,\ \gamma_A)\,, \qquad \Delta\beta_A = \int_{\gamma(t)}^{\gamma_A} \Lambda(\gamma)\,d\gamma\,,$$

$$\eta_A = \frac{1}{\Delta t}\,\frac{\partial F}{\partial \dot{\gamma}} + \frac{\partial F}{\partial \gamma}\,, \qquad \Lambda_A = \Lambda(\gamma_A)\,. \tag{5.7.49a-e}$$

Step 8

Estimate the error in the plastic strain increment and correct the increments in the plastic strain and the backstress,

$$\Delta\gamma_{er} = \frac{\tau_A - \tau^e + \Delta\beta_A}{\mu + \Lambda_A + \eta_A},$$

$$\Delta\gamma = \max\{0,\ \Delta\gamma_A - \Delta\gamma_{er}\},$$

$$\Delta\beta = \begin{cases} 0 & \text{for } \Delta\gamma = 0 \\ \Delta\beta_A - \Lambda_A \Delta\gamma_{er} & \text{for } \Delta\gamma \neq 0 \end{cases}. \qquad (5.7.50a\text{-}c)$$

Step 9

Obtain the final values of the equivalent plastic strain, total stress, and the backstress,

$$\gamma(t+\Delta t) = \gamma(t) + \Delta\gamma,$$

$$\hat{\boldsymbol{\tau}}(t+\Delta t) = \left(1 - \frac{\mu\,\Delta\gamma}{\tau^{tr}}\right)\hat{\mathbf{s}}^{tr} + \hat{\boldsymbol{\beta}}(t),$$

$$\hat{\boldsymbol{\beta}}(t+\Delta t) = \hat{\boldsymbol{\beta}}(t) + \Delta\beta\,\frac{\hat{\mathbf{s}}^{tr}}{\tau^{tr}}. \qquad (5.7.51a\text{-}c)$$

Example: As an illustration, consider the power law for the isotropic flow-stress

$$\tau = \tau_c\,(1 + \gamma/\gamma_0)^N\,(\dot\gamma/\dot\gamma_0)^m, \qquad (5.7.52a)$$

with $\tau_c = \mu/100$, $\gamma_0 = 0.005$, $N = 0.1$, and $\dot\gamma_0 = 0.0001$. As an example consider the following time history for the corotational deformation rate $\hat{\mathbf{D}}$:

$$\hat{\mathbf{D}} = \begin{bmatrix} 1 & 0 & 0 \\ 0 & -1 & 0 \\ 0 & 0 & 0 \end{bmatrix} \times 10^{-2}, \quad 0 \le t < 50,$$

$$\hat{\mathbf{D}} = \frac{1}{\sqrt{2}}\begin{bmatrix} 1 & 1 & 0 \\ 1 & -1 & 0 \\ 0 & 0 & 0 \end{bmatrix} \times 10^{-4}, \quad 50 \le t < 5050,$$

$$\hat{\mathbf{D}} = \frac{1}{\sqrt{2}}\begin{bmatrix} -1 & 0 & 0 \\ 0 & 1 & 1 \\ 0 & 1 & 0 \end{bmatrix} \times 10^{-2}, \quad 5050 \le t < 5100. \qquad (5.7.52b\text{-}d)$$

The components of the deviatoric stress $\hat{\boldsymbol{\tau}}'$ obtained using the *generalized radial-return method* with various numbers of timesteps are shown in Figures 5.7.3 and 5.7.4 for m = 0.01 and m = 0.05, respectively. It is seen in Figure 5.7.3 that when the rate sensitivity is low, the *generalized radial-return method* gives very accurate results for the effective stress. However, the stress components are not very accurate when there is any rotation in the stress orientation. To improve the calculation of the stress orientation, consider the following alternative to the radial-return method.

Perfect-plasticity Path: Alternative to the *radial-return* method is the perfect-

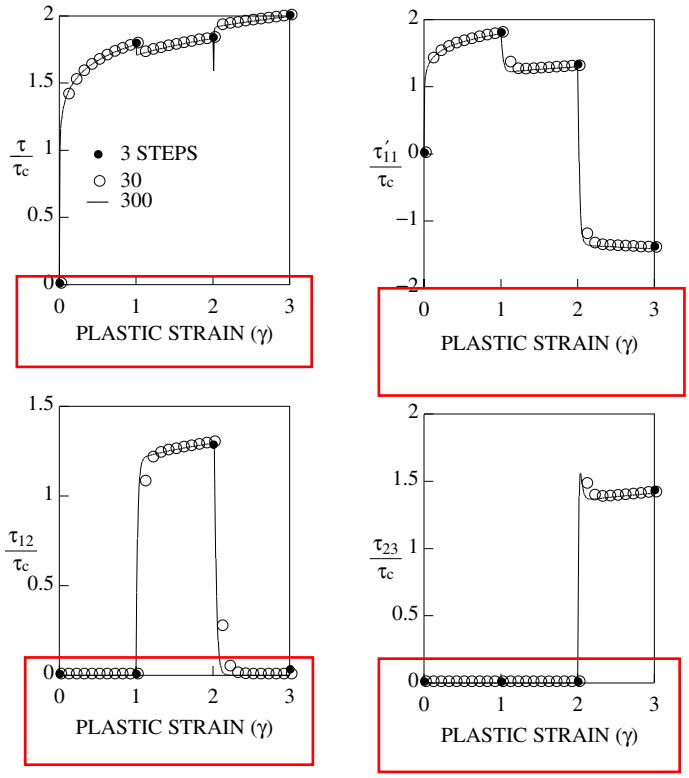

Figure 5.7.3

Time history of deviatoric stress components for rate-dependent plasticity model (5.7.52a) with m = 0.01, and deformation history (5.7.52b-d), using the *generalized radial-return method*

plasticity assumption. However, unlike for the rate-independent flow, there may be no yield surface for the rate-dependent flow[27]. On the other hand, most rate-dependent materials undergo very little plastic deformation when the effective shear stress is less than a reference stress. Hence, in addition to the flow rule (5.7.36), it may be assumed that

$$\dot{\gamma} \ << \ d \quad \text{for} \ \ \tau < \tau_d \equiv F(d, \gamma)\,. \tag{5.7.53a}$$

This also implies that

$$\dot{\gamma} >> d\,, \quad \text{for} \ \ \tau > \tau_d\,. \tag{5.7.53b}$$

Condition (5.7.53) shows that the elastic deformation dominates when $\tau < \tau_d$

[27] Some authors have introduced rate-dependent plastic deformation models with a yield condition, as discussed in Subsection 4.3.2 of Chapter 4.

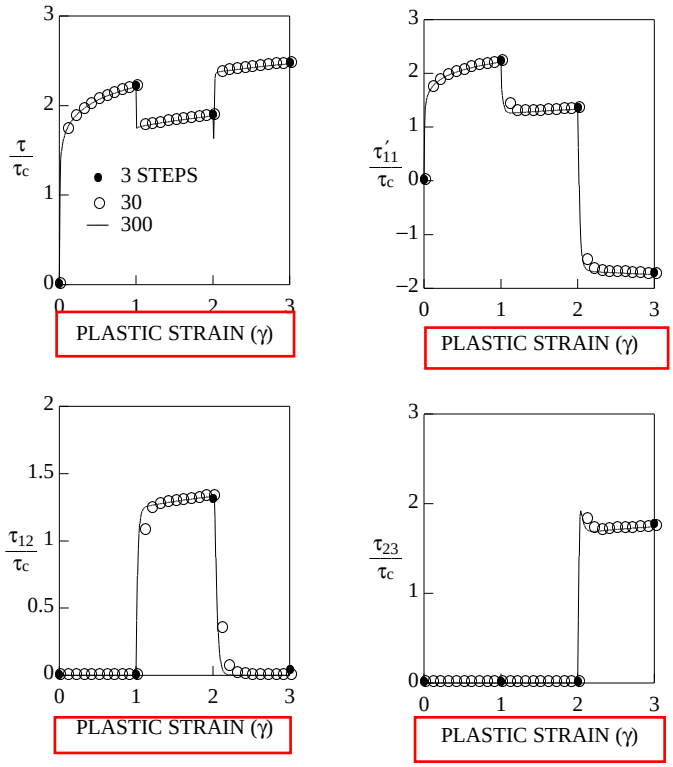

Figure 5.7.4

Time history of deviatoric stress components for rate-dependent plasticity model (5.7.52a) with m = 0.05, and deformation history (5.7.52b-d), using the *generalized radial-return method*

and hence, the stress state moves mostly parallel to the direction of $\hat{\mathbf{D}}$ in the deviatoric stress space. On the other hand, when $\tau > \tau_d$, the plastic deformation dominates, and hence the stress state moves mostly in the direction of $\hat{\boldsymbol{\mu}}$ in the deviatoric stress space. Only if $\tau \approx \tau_d$, then the stress state moves in the direction normal to $\hat{\boldsymbol{\mu}}$. Therefore, the perfect-plasticity-path assumption is reasonable only after the stress magnitude attains the value τ_d.

Denote by Δt^e the time that is taken for the effective stress to reach the value τ_d. This depends on whether the initial effective stress $\tau(t)$ is greater or less than τ_d. Note that, even if $\tau(t)$ is greater than τ_d, because of the dominant plastic deformation, the effective stress drops to τ_d, regardless of whether it is loading ($\hat{\mathbf{D}} : \hat{\boldsymbol{\mu}} > 0$) or unloading ($\hat{\mathbf{D}} : \hat{\boldsymbol{\mu}} < 0$).

Consider the integration of (5.3.13a) and (5.3.13d) from time $t^e = t + \Delta t^e$ to $t^e + \Delta t^p$, where $\Delta t^p = \Delta t - \Delta t^e$. Assume that $\tau(t^e) \approx \tau_d$. See Subsection 5.7.4 for

the evaluation of Δt^e and $\boldsymbol{\tau}(t^e)$. In this timestep, (5.3.13a) reduces to (5.7.24). Then the orientation of the stress difference, $\hat{\boldsymbol{\mu}}(t^e + \xi)$, is given by (5.7.25a).

Now, consider the integration of (5.7.22), using the *plastic-predictor/elastic-corrector* method. In this method, first estimate the plastic deformation rate by

$$\dot{\gamma}_A(\xi) = d\,x(\xi)\,. \tag{5.7.54a}$$

Then, in view of (5.7.25b), the increment of plastic strain is estimated as

$$\Delta\gamma_A(\xi) = \frac{d}{A}\,ln\,(z(\xi))\,. \tag{5.7.54b}$$

The errors in the estimated plastic strain rate and the increment of plastic strain are assumed to be related by

$$\dot{\gamma}(\xi) = \dot{\gamma}_A(\xi) - \dot{\gamma}_{er}\,, \qquad \Delta\gamma(\xi) = \Delta\gamma_A(\xi) - \Delta\gamma_{er}\,,$$
$$\dot{\gamma}_{er} = \Delta\gamma_{er}/\Delta t\,. \tag{5.7.55a-c}$$

Integration of (5.7.28b), in view of (5.7.54) and (5.7.55), results in

$$\tau(t^e + \Delta t^p) = \tau(t^e) + \Delta\beta_A + (\mu + \Lambda_A)\,\Delta\gamma_{er}\,, \tag{5.7.56a}$$

where

$$\Delta\beta_A \equiv \int_{\gamma(t)}^{\gamma_A} \Lambda(\gamma)\,d\gamma\,, \qquad \gamma_A \equiv \gamma(t) + \Delta\gamma_A(\Delta t)\,, \qquad \Lambda_A \equiv \Lambda(\gamma_A)\,. \tag{5.7.56b-d}$$

A Taylor series expansion of the flow rule at $(\dot{\gamma}_A(\Delta t),\ \gamma_A)$ gives

$$\tau(t^e + \Delta t^p) = \tau_A - \eta_A\,\Delta\gamma_{er}\,, \tag{5.7.57a}$$

where

$$\tau_A \equiv F(\dot{\gamma}_A(\Delta t),\ \gamma_A)\,, \qquad \eta_A \equiv \frac{1}{\Delta t}\,\frac{\partial F}{\partial \dot{\gamma}} + \frac{\partial F}{\partial \gamma}\,. \tag{5.7.57b,c}$$

Substitute (5.7.57a) into (5.7.56a), to obtain

$$\Delta\gamma_{er} = \frac{\tau_A - \tau(t^e) + \Delta\beta_A}{\mu + \Lambda_A + \eta_A}\,. \tag{5.7.58}$$

Finally, the values of the stress difference and the backstress are given by

$$\hat{\mathbf{s}}\,(t^e + \Delta t^p) = \tau(t^e + \Delta t^p)\,\hat{\boldsymbol{\mu}}(t^e + \Delta t^p)\,,$$
$$\hat{\boldsymbol{\beta}}(t^e + \Delta t^p) = \hat{\boldsymbol{\beta}}(t^e) + \sqrt{2}\,(\Delta\beta_A - \Lambda_A\,\Delta\gamma_{er})\,\hat{\boldsymbol{\mu}}(t^e + \Delta t^p)\,. \tag{5.7.59a,b}$$

Computational Steps: The necessary computational steps are summarized below.

Step 1

Obtain the initial values of the stress difference and the dynamic critical stress,

$$\hat{\mathbf{s}}(t) = \hat{\boldsymbol{\tau}}(t) - \hat{\boldsymbol{\beta}}(t)\,, \qquad \tau_t \equiv \tau(t) = \{\tfrac{1}{2}\,\hat{\mathbf{s}}(t) : \hat{\mathbf{s}}(t)\}^{\frac{1}{2}}\,,$$

$$z_1 = \sinh(A\,\Delta t^p) + k\cosh(A\,\Delta t^p) - k\,,$$

$$\hat{\boldsymbol{\mu}}(t+\Delta t) = \frac{1}{\sqrt{2}\,z\,\tau(t^e)}\,\hat{\mathbf{s}}(t^e) + \frac{\sqrt{2}\,z_1}{z\,d}\,\hat{\mathbf{D}}\,. \qquad (5.7.63a\text{-}f)$$

Step 7

Estimate the plastic strain rate, plastic strain, flow stress, increment in the back stress, and the hardening moduli at the end of the timestep,

$$\dot{\gamma}_A = \max\{\sqrt{2}\,\hat{\boldsymbol{\mu}}(t+\Delta t) : \hat{\mathbf{D}}\,,\, 0\}\,, \quad \Delta\gamma_A = \frac{1}{A}\,d\,ln\,(z)\,,$$

$$\gamma_A = \gamma(t) + \Delta\gamma_A\,, \quad \tau_A = F(\dot{\gamma}_A,\ \gamma_A)\,, \quad \Delta\beta_A = \int_{\gamma(t)}^{\gamma_A} \Lambda(\gamma)\,d\gamma\,,$$

$$\Lambda_A = \Lambda(\gamma_A)\,, \quad \eta_A = \frac{1}{\Delta t}\,\frac{\partial F}{\partial \dot{\gamma}}(\dot{\gamma}_A,\ \gamma_A) + \frac{\partial F}{\partial \gamma}(\dot{\gamma}_A,\ \gamma_A)\,. \qquad (5.7.64a\text{-}g)$$

Step 8

Estimate the error in the estimated plastic strain increment, and obtain the final values of the equivalent plastic strain, the stress difference, the backstress, and the total stress,

$$\Delta\gamma_{er} = \frac{\tau_A - \tau(t^e) + \Delta\beta_A}{\mu + \eta_A + \Lambda_A}\,,$$

$$\gamma(t+\Delta t) = \gamma_A - \Delta\gamma_{er}\,,$$

$$\tau(t+\Delta t) = \tau(t^e) - \Delta\beta_A + (\mu + \Lambda_A)\,\Delta\gamma_{er}\,,$$

$$\hat{\mathbf{s}}(t+\Delta t) = \sqrt{2}\,\tau(t+\Delta t)\,\hat{\boldsymbol{\mu}}(t+\Delta t)\,,$$

$$\hat{\boldsymbol{\beta}}(t+\Delta t) = \hat{\boldsymbol{\beta}}(t) + \sqrt{2}\,(\Delta\beta_A - \Lambda_A\,\Delta\gamma_{er})\,\hat{\boldsymbol{\mu}}(t+\Delta t)\,,$$

$$\hat{\boldsymbol{\tau}}(t+\Delta t) = \hat{\mathbf{s}}(t+\Delta t) + \hat{\boldsymbol{\beta}}(t+\Delta t)\,. \qquad (5.7.65a\text{-}f)$$

The stress components obtained using the *perfect-plasticity-path method* for the same example in Figures 5.7.3 and 5.7.4, with various numbers of timesteps, are shown in Figures 5.7.5 and 5.7.6, for $m = 0.01$ and $m = 0.05$ respectively. Essentially exact results are obtained for any number of timesteps, from 3 to 300.

5.7.4. Elasticity-dominated Deformation

In the previous two subsections, the *perfect-plasticity-path* method is used when the deformation is dominated by plastic deformation. In rate-independent plasticity, the deformation is regarded elastic in unloading and when the effective stress difference is less than the current value of the yield stress. In the rate-dependent case with strain-rate softening or hardening, the stress path deviates from the perfect-plasticity path even in loading. In that case, both elastic and plastic deformations are involved essentially in all time increments.

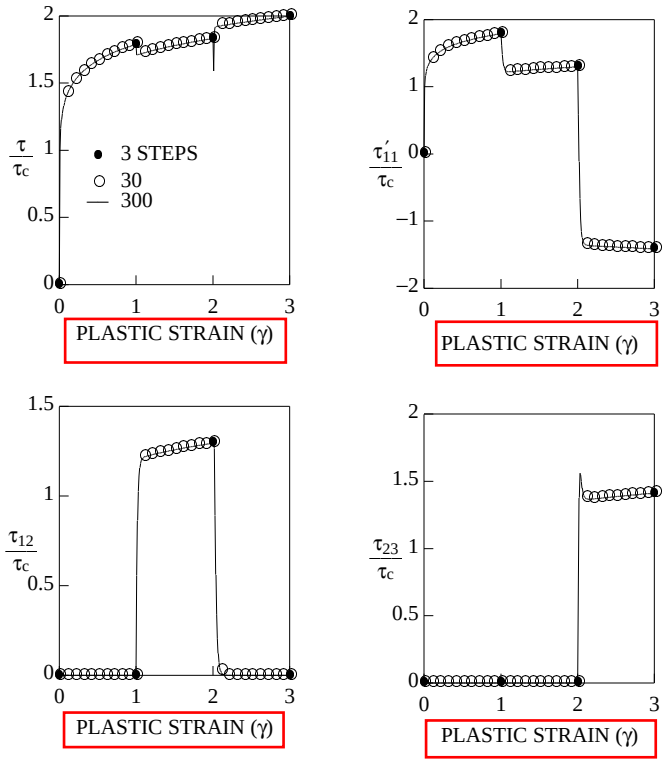

Figure 5.7.5

Time history of deviatoric stress components for rate-dependent plasticity model (5.7.52a) with m = 0.01, and deformation history (5.7.52b-d), using the *perfect-plasticity-path method*

Rate-independent Model: For rate-independent materials, the deformation is purely elastic if the effective stress is less than the current yield stress. Consider a time increment Δt, and denote by Δt^e, the portion of this time which it takes to reach the yield surface. In this range, the rate of change of the stress difference (5.3.13a) is

$$\mathbf{K} \equiv \overset{\circ}{\hat{\mathbf{s}}} = 2\mu\,\hat{\mathbf{D}}\,. \tag{5.7.66a}$$

Therefore, the duration of the elastic deformation, Δt^e, is obtained from

$$(\hat{\mathbf{s}}_t + \mathbf{K}\,\Delta t^e) : (\hat{\mathbf{s}}_t + \mathbf{K}\,\Delta t^e) = 2\,\tau_y^2 \tag{5.7.66b}$$

which yields

$$\Delta t^e = \min\left\{\Delta t\,,\ \frac{\sqrt{(\hat{\mathbf{s}}_t : \mathbf{K})^2 + 2\,\mathbf{K} : \mathbf{K}\,(\tau_y^2 - \tau_t^2)} - \hat{\mathbf{s}}_t : \mathbf{K}}{\mathbf{K} : \mathbf{K}}\right\}, \tag{5.7.66c}$$

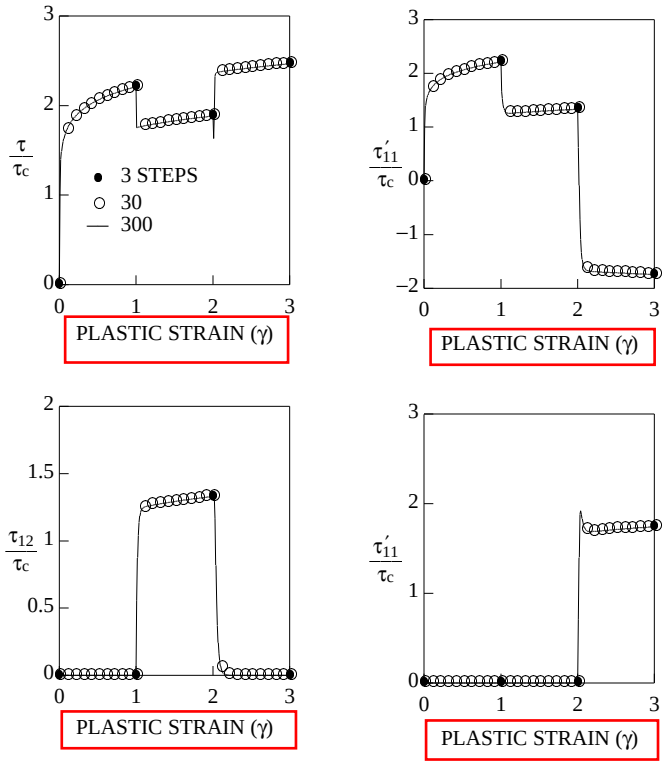

Figure 5.7.6

Time history of deviatoric stress components for rate-dependent plasticity model (5.7.52a) with m = 0.05, and deformation history (5.7.52b-d), using the *perfect-plasticity-path method*

where $\hat{\mathbf{s}}_t = \hat{\mathbf{s}}(t)$. The stress difference at the end of the period of the elastic deformation is obtained as follows:

$$\hat{\mathbf{s}}(t + \Delta t^e) = \hat{\mathbf{s}}(t) + \mathbf{K}\,\Delta t^e\,. \tag{5.7.66d}$$

The timestep during which plastic deformation is dominant is then given by

$$\Delta t^p = \Delta t - \Delta t^e\,. \tag{5.7.66e}$$

Rate-dependent Model: In the case of rate-dependent materials, there is no yield surface. However, if a material element is subjected to a constant deformation rate for a relatively long time, in the absence of strain hardening, the effective stress difference would reach a value τ_d, given by

$$\tau_d \equiv F(d,\ \gamma(t))\,. \tag{5.7.67}$$

Step 10

Estimate the error in the estimated plastic strain increment and correct the increments in the plastic strain and the backstress,

$$\Delta\gamma_{er} = \frac{\tau_A - \tau^e + \Delta\beta_A}{\mu + \Lambda_A + \eta_A}, \quad \Delta\gamma = \max\{0,\ \Delta\gamma_A - \Delta\gamma_{er}\},$$

$$\Delta\beta = \begin{cases} 0 & \text{for } \Delta\gamma = 0 \\ \Delta\beta_A - \Lambda_A \Delta\gamma_{er} & \text{for } \Delta\gamma \neq 0 \end{cases}. \qquad (5.8.63a\text{-}c)$$

Step 11

Obtain the final values of the equivalent plastic strain, total stress, and the backstress,

$$\gamma(t+\Delta t) = \gamma(t) + \Delta\gamma, \quad \boldsymbol{\tau}^{\theta}(t+\Delta t) = \left(1 - \frac{\mu\,\Delta\gamma}{\tau^{tr}}\right)\mathbf{s}^{tr} + \boldsymbol{\beta}(t),$$

$$\boldsymbol{\beta}^{\theta}(t+\Delta t) = \boldsymbol{\beta}(t) + \Delta\beta\,\frac{\mathbf{s}^{tr}}{\tau^{tr}}. \qquad (5.8.64a\text{-}c)$$

As an illustration, consider the isotropic power-law hardening model (5.7.38), and consider the following piecewise constant velocity gradient:

$$\mathbf{L} = \begin{bmatrix} 1 & 0 & 0 \\ 0 & -1 & 0 \\ 0 & 0 & 0 \end{bmatrix} \times 10^{-2}, \quad 0 \le t < 50,$$

$$\mathbf{L} = \begin{bmatrix} 0.707 & -99.707 & 0 \\ 100.707 & -0.707 & 0 \\ 0 & 0 & 0 \end{bmatrix} \times 10^{-4}, \quad 50 \le t < 100,$$

$$\mathbf{L} = \begin{bmatrix} -0.707 & 0 & 0 \\ 0 & 0.707 & 1.707 \\ 0 & -0.293 & 0 \end{bmatrix} \times 10^{-2}, \quad 100 \le t < 150. \qquad (5.8.65a\text{-}c)$$

In this example, the strain-rate sensitivity parameter m = 0.05 is used. The components of the deviatoric stress $\boldsymbol{\tau}'$, obtained by using the *generalized radial-return method* with various numbers of timesteps, are shown in Figure 5.8.4. As is seen, the *generalized radial-return method* gives accurate results even with large timesteps when the rotation is of the order of the distortion. However, when the rotation is orders of magnitude larger than the distortion, small timesteps are required for accurate results. To improve the results for large rotations, as an alternative to the *generalized radial-return method*, consider the *perfect-plasticity path method*. The computational steps for this method are given in the following:

Computational Steps for the Perfect-plasticity Path Method:

Step 1

Obtain the initial values of the stress difference and the dynamic critical stress,

$$\mathbf{s}(t) = \boldsymbol{\tau}(t) - \boldsymbol{\beta}(t), \quad \tau(t) = \{\tfrac{1}{2}\,\mathbf{s}(t) : \mathbf{s}(t)\}^{1/2},$$

Another interesting feature of this experiment is the formation of tension cracks at four locations in the interior surface of the collapsed cylinder. Dynamic void collapse and void growth in single crystals under uniaxial loads have been studied analytically by Nemat-Nasser and Hori (1987), revealing that tension cracks may be produced (even in a ductile material) during unloading, in a direction normal to the applied compression, even if the sample has not been subjected to any externally applied tensile stresses. This prediction has been verified experimentally by Nemat-Nasser and Chang (1990) for single-crystal copper as well as other metals, *e.g.*, mild steel and iron, using a split Hopkinson bar dynamic loading technique. A similar phenomenon occurs in the cylinder-collapse experiment. This is also verified by computational modeling which shows that very high tensile stresses can develop at certain critical points on and near the inside surface of the collapsed cylinder. This and many other issues relating to anisotropic deformation of thick-walled cylinders of single-crystal copper, under initially uniform dynamic loading, are discussed in Nemat-Nasser *et al.* (1998d), where the effect of the initial crystal orientation on the final collapsed geometry is studied by numerical simulation.

6.5.14. Dislocation-based Model for bcc and fcc Crystals

In this case, use constitutive relation (6.5.18) for the fcc-case, and then simply set $a_0 = 0$ to obtain the necessary equations for the bcc-case. To simplify calculations, rewrite (6.5.18) as

$$\tau^\alpha = \tau_a + \Psi^\alpha, \qquad \Psi^\alpha = \hat{\tau}_0\, f\,[1 - X^{1/q}]^{1/p},$$

$$f = \begin{cases} 1 + a_0\,[1 - (T/T_m)^2]\,\gamma^n & \text{for fcc} \\ 1 & \text{for bcc} \end{cases},$$

$$X = -\frac{k\,T}{G_0}\, ln\frac{\dot{\gamma}^\alpha f}{\dot{\gamma}_0} \qquad \text{(6.5.50a-d)}$$

Hence, it is assumed that the athermal stress is the same for all slip systems, and that its dependence on slip is only through the total accumulated slip, γ, defined by (6.5.1e). Now, using the chain rule of differentiation, coefficients in (6.5.41a) are easily evaluated.

To this end, note that

$$\frac{\partial \tau_a}{\partial \gamma} = \frac{n_1}{\gamma}\,(\tau_a - c_0), \qquad \frac{\partial f}{\partial \gamma} = \frac{n}{\gamma}\,(f - 1),$$

$$\frac{\partial f}{\partial T} = -2a_0\,(T/T_m^2)\,\gamma^n, \qquad \frac{\partial X}{\partial \gamma} = \frac{-k\,T}{G_0\,f}\,\frac{\partial f}{\partial \gamma},$$

$$\frac{\partial X}{\partial T} = \frac{X}{T} - \frac{k\,T}{G_0\,f}\,\frac{\partial f}{\partial T}, \qquad \frac{\partial X}{\partial \dot{\gamma}^\alpha} = -\frac{k\,T}{G_0\,\dot{\gamma}^\alpha}.$$

$$\frac{\partial \Psi^\alpha}{\partial X} = -\frac{\hat{\tau}_0\, f}{p\,q}\,[1 - X^{1/q}]^{\frac{1-p}{p}}\, X^{\frac{1-q}{q}}. \qquad \text{(6.5.51a-g)}$$

geometric line defects in crystals, produces inelastic strains accompanied by an accommodating elastic lattice distortion, leading to a compatible total deformation. Indeed, since interatomic forces cannot support large elastic distortions of the lattice, dislocations are generated to relieve the elastic deformation and to minimize the associated elastic energy of the crystal. In essentially all known crystalline materials, the lattice elastic strains are infinitesimally small, being of the order of 10^{-3}. The plastic strains associated with the dislocations that are present in a crystal, are also very small. Therefore, large plastic deformations of crystals occur by the motion of dislocations that are constantly generated and annihilated, as atoms rearrange and matter *flows* through the lattice, and not by a continuous storage of dislocations. For example, an annealed cylindrical sample of copper of centimeter dimensions, can be deformed, say, at a 600K temperature, to a thin sheet of submillimeter thickness, while its final dislocation density is about the same as that of its initial undeformed state, *i.e.*, about $10^7\,\mathrm{cm}^{-2}$. A three-orders of magnitude increase in this dislocation density, means an average dislocation spacing of about 0.1μm, which is rather small, but does not correspond to significant plastic strains.

It is therefore essential to clearly distinguish between the *total plastic deformation* of a crystalline solid, which can be hundreds or even thousands of percent, and *the plastic strains due to the presence of dislocations within a crystalline solid*, which generally is very small, of the order of the associated elastic strains. While the analysis of the total finite deformation of crystals must be performed within a fully nonlinear setting, as discussed in Section 6.2, small deformation, linearized kinematics is generally sufficient to deal with the elasto-plastic deformation due to the existing dislocations within crystals or polycrystals.[78]

In view of the above comments, it is generally unnecessary to distinguish between the configurations of a crystal without and with dislocations, *i.e.*, the particle positions in an *undislocated* and in the corresponding *dislocated crystal* are indistinguishable. The displacement gradient field, $\boldsymbol{\nabla}\otimes\mathbf{u} = u_{i,j}(\mathbf{x})\,\mathbf{e}_j\otimes\mathbf{e}_i$, of a dislocated crystal may thus be additively split into an elastic, $\boldsymbol{\beta}^e$, and a plastic, $\boldsymbol{\beta}^p$ (due to the presence of dislocations), part,

$$(\boldsymbol{\nabla}\otimes u)^T = \boldsymbol{\beta}^e + \boldsymbol{\beta}^p\,,$$
$$u_{i,j} = \beta^e_{ij} + \beta^p_{ij}\,. \tag{6.5.62a}$$

The plastic part, $\boldsymbol{\beta}^p$, is associated with the dislocations that are present on various slip planes of the crystal or the crystals in a polycrystal. The dislocation density tensor is now defined by Kröner's equation,[79]

---

[78] The shear strain that produced the shearband in Figure 6.5.12a is about 910%, while the residual plastic (and elastic) strains due to the dislocations that remain in the material (Figure 6.5.12b), are fractions of one percent.

[79] See Mura (1987, page 53). Note that Mura defines the positive direction of the normal to the S^+ towards the S^-, whereas in the present work the opposite direction is used; see Figure 6.1.7, page 392. Hence, the minus sign in Mura's formula.

corresponding three reciprocal vectors, say, $\mathbf{b}^i$; see Subsection 1.3.1, page 19. The lattice vectors and their reciprocals are related by

$$\mathbf{a}_i \cdot \mathbf{b}^j = \delta_i^j \,. \tag{6.A.1a}$$

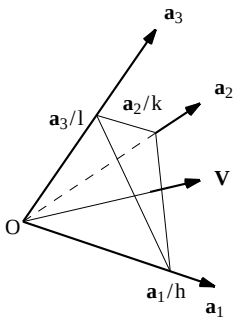

Figure 6.A.1

A unit cell defined by lattice vectors $\mathbf{a}_i$, i = 1, 2, 3, and the plane (hkl) normal to $\mathbf{V} = h\,\mathbf{b}^1 + k\,\mathbf{b}^2 + l\,\mathbf{b}^3$

Hence, it follows that

$$\mathbf{b}^1 = \frac{\mathbf{a}_2 \times \mathbf{a}_3}{V} \,,$$

$$\mathbf{b}^2 = \frac{\mathbf{a}_3 \times \mathbf{a}_1}{V} \,,$$

$$\mathbf{b}^3 = \frac{\mathbf{a}_1 \times \mathbf{a}_2}{V} \,, \tag{6.A.1b-d}$$

where $V = \mathbf{a}_1 \cdot \mathbf{a}_2 \times \mathbf{a}_3$ is the volume of the unit cell formed by the lattice vectors. With the aid of permutation symbol, e_{ijk}, (6.A.1b-d) are more concisely written as,

$$\mathbf{b}^i = \frac{1}{2\,V}\, e_{ijk}\, \mathbf{a}_j \times \mathbf{a}_k \,,$$

$$\mathbf{a}_i \times \mathbf{a}_j = V\, e_{ijk}\, \mathbf{b}^k \,. \tag{6.A.1e,f}$$

Miller Indices for Directions: A direction can be defined by a vector, say **v**, through the origin of the unit cell. Let v_i define the components of this vector in the lattice coordinates,

$$\mathbf{v} = v_1\,\mathbf{a}_1 + v_2\,\mathbf{a}_2 + v_3\,\mathbf{a}_3 \,. \tag{6.A.2a}$$

In general, these components need not be integers or even rational numbers. In application to crystals, however, it is generally assumed that the directions of interest can be defined with rational components. Hence, multiplying the vector **v** by the least common denominator of its (rational) components, say m, a new vector $m\,\mathbf{v}$ is obtained which has integer components,

$$m\,v_1 = u \,, \quad m\,v_2 = v \,, \quad m\,v_3 = w \,, \tag{6.A.2b-d}$$